



## Research Article

# On the Impact of the LHC Run 2 Data on General Composite Higgs Scenarios

Charanjit K. Khosa <sup>1,2</sup> and Veronica Sanz <sup>3,4</sup>

<sup>1</sup>Dipartimento di Fisica, Università di Genova and INFN, Sezione di Genova, Via Dodecaneso 33, 16146, Italy

<sup>2</sup>H.H. Wills Physics Laboratory, University of Bristol, Tyndall Avenue, Bristol BS8 1TL, UK

<sup>3</sup>Department of Physics and Astronomy, University of Sussex, BN1 9QH Brighton, UK

<sup>4</sup>Instituto de Física Corpuscular (IFIC), Universidad de Valencia-CSIC, E-46980 Valencia, Spain

Correspondence should be addressed to Veronica Sanz; [v.sanz@sussex.ac.uk](mailto:v.sanz@sussex.ac.uk)

Received 25 June 2021; Accepted 22 January 2022; Published 9 February 2022

Academic Editor: Grégory Moreau

Copyright © 2022 Charanjit K. Khosa and Veronica Sanz. This is an open access article distributed under the Creative Commons Attribution License, which permits unrestricted use, distribution, and reproduction in any medium, provided the original work is properly cited. The publication of this article was funded by SCOAP<sup>3</sup>.

We study the impact of Run 2 LHC data on general composite Higgs scenarios, where nonlinear effects, mixing with additional scalars, and new fermionic degrees of freedom could simultaneously contribute to the modification of Higgs properties. We obtain new experimental limits on the scale of compositeness, the mixing with singlets and doublets with the Higgs, and the mass and mixing angle of top-partners. We also show that for scenarios where new fermionic degrees of freedom are involved in electroweak symmetry breaking, there is an interesting interplay among Higgs coupling measurements, boosted Higgs properties, SMEFT global analyses, and direct searches for single and double production of vector-like quarks.

## 1. Introduction

The true origin of the Higgs mechanism is still an open question in Particle Physics, despite the discovery of its key element, the Higgs particle [1, 2], and the observation of the SM-like nature of its couplings to massive particles [3].

The main reason to doubt a purely SM Higgs sector can be traced back its quantum behaviour, a problem often expressed in the context of *naturalness*: how can a fundamental scalar be so light, yet so sensitive to UV effects. And this is not the only suspicious aspect of the SM Higgs. The hierarchy among its Yukawa couplings or its inability to produce enough baryon asymmetry during the electroweak phase transition also add to the unsatisfactory aspects of the SM Higgs sector.

However, these shortcomings also open opportunities for new physics. The Higgs, due to its scalar nature, could connect to other sectors via mixing with scalars and participate in phase transitions and inflation. Among the theories bringing the Higgs into a new framework, one particularly

appealing proposal is the concept of compositeness, leading to composite Higgs models (CHMs). In CHMs, the Higgs is not a truly fundamental particle but a bound state of other, more fundamental, particles.

Primitive proposals for a composite Higgs [4, 5] were replaced by more realistic realisations based on the idea that a Higgs is not just any composite state from strong dynamics, but a pseudo-Goldstone boson [6, 7]. Pseudo-Goldstone bosons appear when approximate global symmetries are spontaneously broken. The size of the symmetry and what it breaks down to determines the amount of scalar degrees of freedom one will have in CHMs. The partial gauging of some of these global symmetries sets what kinds of quantum numbers the scalars have. The minimal framework to achieve successful electroweak symmetry breaking (EWSB), i.e., leading to a Higgs doublet of  $SU(2)_L$  with a  $m_h \sim v$ , was found in Ref. [4, 5]. In this setup, the Higgs originated from the breaking  $SO(5) \rightarrow SO(4)$ , and its radiative potential had to be supplemented with a new vector-like fermion with the same quantum numbers as the top, called *top-*

partner and denoted by  $T$ . This minimal set-up and its phenomenological consequences have been thoroughly explored in the literature, see, e.g., Ref. [8] for a review.

Typically, one would assume the main manifestation of the composite nature of the Higgs would be the nonlinear origin of its couplings, leading to very specific types of Higgs coupling deviations. Yet, composite Higgs scenarios could exhibit a richer phenomenology, such as the presence of new scalars or fermions which would also modify the Higgs properties. The focus of this paper is the study of the rich patterns which arise in general composite Higgs scenarios and what the Run 2 LHC data can tell us about them. The data we will use for this analysis is summarised in Table 1.

The paper is organised as follows. In Section 2, we describe the different patterns arising in composite Higgs scenarios: nonlinear effects (Section 2.1), extended scalar sectors (Section 2.2), and new fermionic degrees of freedom (Section 2.3). In these sections, we examine the impact that Higgs measurements and direct top-partner searches have on these patterns and in combinations of them, e.g., how nonlinearities and mixing with new scalars do contribute on the same direction to reduce Higgs couplings to massive particles. Hence, as one switches on more than one of these effects, each individual limit becomes stronger. Section 3 is devoted to conclusions.

## 2. Patterns of Composite Higgs Scenarios

The idea of the Higgs as a composite state could be realised in many ways. Considering that theoretical constraints and precision measurements substantially reduce the possible scenarios, yet there are still many possibilities to contemplate. Nevertheless, one can describe modern composite Higgs scenarios as exhibiting one or more of the following patterns:

- (1) A composite Higgs sector would be able to trigger electroweak symmetry in a nonlinear fashion. This leads to new possibilities for the light Higgs boson. Its couplings, and even quantum numbers, could be different from the SM expectation. Indeed, in the SM the Higgs is a  $SU(2)_L$ -doublet, and the way it induces EWSB completely determines how it couples to fermions and bosons, including couplings to more than one Higgs. On the other hand, in CHMs, these couplings would be more general, even opening the possibility of a  $SU(2)_L$  singlet Higgs [22, 23]. This additional freedom leads to the expectation that the SM-like Higgs, the 125 GeV state observed by the CERN collaborations, should exhibit nonstandard interactions. We will discuss this first composite Higgs pattern in Section 2.1
- (2) The second set of patterns found in CHMs refers to the origin of the composite Higgs in the spontaneous breaking of an approximate global symmetry. This breaking could lead to *just* the right amount of degrees of freedom to match one single light Higgs particle and the three missing polarisations of the

TABLE 1: Experimental measurements considered in this work.

Measurement	Reference
Higgs measurements	
Run 1 ATLAS and CMS combined Higgs signal strength measurements	[9]
Run 2 ATLAS Higgs signal strength measurements	[10, 11]
Run 2 CMS Higgs signal strength measurements	[12–16]
ATLAS Higgs+jet differential measurement	[17]
LHC direct searches for VLQ	
ATLAS $T \rightarrow Wb$ channel	[18]
ATLAS $T \rightarrow \text{top} + \text{MET}$ channel	[19]
CMS $T \rightarrow Wb$ channel	[20]
CMS $T \rightarrow Zt$ final state	[21]

$W^\pm$  and  $Z$  bosons. But, more generically, this breaking would lead to new scalar degrees of freedom which, after partially gauging the global symmetry, could be identified as  $SU(2)_L$  singlets, doublets, or even higher representations. These nonminimal coset embeddings would lead to additional degrees of freedom which could also develop their own potential, participate in EWSB, and typically mix with the SM-like Higgs. As we have not observed more scalars than the Higgs, these additional scalars would be typically required to be heavier than the Higgs. Therefore, their indirect effects could appear through virtual corrections to the Higgs couplings. At leading order, the effects could be at tree level in the effective theory via mixing with the SM-like Higgs. The study of the Run 2 limits on these extensions of the SM scalar sector can be found on Section 2.2. Note that the additional pseudo-Goldstone degrees of freedom would exhibit their own phenomenology in the form of the so-called axion-like particles (ALPs), see Ref. [24] for a brief introduction to ALPs. The same parameter  $f$  which we will constrain using the Higgs couplings would also influence the ALP phenomenology, see, e.g., Refs. [25–30]

- (3) The third set of patterns found in CHMs refers to the presence of new, fermionic degrees of freedom which would assist the SM-like Higgs in its job of triggering EWSB. These fermions, often called top-partners, should be relatively light to efficiently modify the Higgs potential. They can be searched for directly, via their production at the LHC through couplings to the strong or electroweak sector, or indirectly, as they modify the Higgs properties. The discussion on direct and indirect searches for top-partners will be developed in Section 2.3
- (4) In each section, we also discuss situations where more than one dominant pattern could be at play in the LHC measurements. We will explain how in this case, their effect in the Higgs couplings would go in the same direction, ruling out cancellations

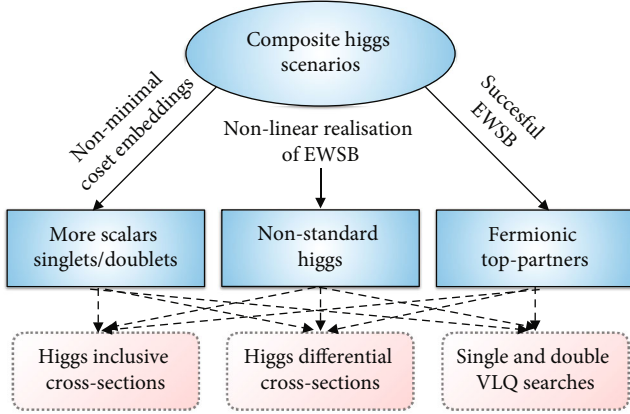


FIGURE 1: Different realisations of composite Higgs scenario and the relevant experimental measurements.

which could invalidate the limits from the previous sections

These patterns are summarised in Figure 1.

**2.1. CHM Pattern I: Nonlinear Effects.** In CHM, one assumes the existence of a global symmetry  $G$ , spontaneously broken to a smaller subgroup  $H$ . The Higgs particle and the would-be Goldstone bosons for the  $W^\pm$  and  $Z$  originate from this breaking. A part of  $H$  is then weakly gauged to provide the Higgs and massive gauge bosons with the correct properties under the SM.

To go beyond the SM structure of EWSB, it is useful to follow the Callan, Coleman, Wess, and Zumino prescription [31]. Within this prescription, one aims to build objects with definite transformation properties under  $SU(2) \times U(1)$ . In CHMs, the object that contains the Goldstones from the global breaking  $G \rightarrow H$  is  $\Sigma = \exp i\phi^a X^a/f$ , where  $\phi^a$  is the Goldstones and  $X^a$  generators in the coset  $G/H$  and  $f$  is the scale associated with the spontaneous breaking. At low energies, below  $f$ , one can write an effective Lagrangian involving  $\Sigma$

$$\mathcal{L}_{\text{kinetic}}^{\text{eff}} = \frac{f^2}{4} \text{Tr} [D_\mu \Sigma^\dagger D^\mu \Sigma], \quad (1)$$

which, after making a choice for weakly gauging  $H$ , determines the Higgs and vector boson interactions. Assuming the Higgs is a doublet of  $SU(2)_L$ , similarly as in the SM, the structure that arises from this kinetic term is

$$g^2 f^2 \sin^2\left(\frac{h}{f}\right). \quad (2)$$

One could also allow the Higgs to be a singlet under  $SU(2)_L$ , but that would lead to the need to impose a tuning in the effective Lagrangian to explain the specific relations between the  $Z$  and  $W$  masses [32, 33]. We will not follow this path in this paper and embed the CHM global symmetry structure in a way that preserves the custodial symmetry present in the SM.

TABLE 2: Summary of CMS Run 2 Higgs signal strength measurements.

Production	Decay channel	Lumi [reference]	Signal strength
ggH	$H \rightarrow ZZ$	137.1 fb <sup>-1</sup> [12]	$0.98^{+0.12}_{-0.11}$
VBF			$0.57^{+0.46}_{-0.36}$
VH			$1.10^{+0.96}_{-0.74}$
$t\bar{t}H, tH$			$0.25^{+1.03}_{-0.25}$
ggH			$0.98^{+0.13}_{-0.10}$
VBF	$H \rightarrow \gamma\gamma$	137 fb <sup>-1</sup> [13]	$1.15^{+0.36}_{-0.31}$
VH			$0.71^{+0.31}_{-0.28}$
$t\bar{t}H$			$1.40^{+0.33}_{-0.27}$
ggF			$1.28^{+0.20}_{-0.19}$
VBF			$0.63^{+0.65}_{-0.61}$
WH	$H \rightarrow WW$	35.9 fb <sup>-1</sup> [12]	$2.85^{+2.11}_{-1.87}$
ZH			$0.90^{+1.77}_{-1.43}$
$t\bar{t}H$			$0.93^{+0.48}_{-0.45}$
ggH			$2.45^{+2.53}_{-2.35}$
WH			$1.27^{+0.42}_{-0.40}$
ZH	$H \rightarrow b\bar{b}$	Up to 77.4 fb <sup>-1</sup> [12]	$0.93^{+0.33}_{-0.31}$
$t\bar{t}H$			$1.13^{+0.33}_{-0.30}$
VBF			$2.53 \pm 1.53$
ggH			$0.98^{+0.20}_{-0.19}$
VBF			$0.67^{+0.23}_{-0.22}$
$t\bar{t}H$	$H \rightarrow \tau\tau$	137 fb <sup>-1</sup> [13]	$0.92^{+0.26}_{-0.23}$
ggH			$0.63^{+0.65}_{-0.64}$
VBF			$1.36^{+0.69}_{-0.61}$
VH			$5.48^{+3.10}_{-2.83}$
$t\bar{t}H$			$2.32^{+2.27}_{-1.95}$

Expanding around the physical Higgs boson vacuum expectation value (VEV), one finds clear predictions of the structure of the Higgs-vector boson couplings

$$\kappa_V = \frac{g_{VVh}^{\text{CH}}}{g_{VVh}^{\text{SM}}} = \sqrt{1 - \xi} \approx 1 - \frac{1}{2}\xi, \quad (3)$$

where  $\xi = v^2/f^2$ .

Turning now to the Higgs-fermion couplings, we note that the predictions are not unique. In particular, the fermion mass generation mechanism in CHMs usually relies on the concept of partial compositeness [32, 34], i.e., the idea that SM fermions feel EWSB via mixing with fermionic bound states. To build structures leading to fermion couplings to the Higgs, one needs to specify the embedding of

TABLE 3: Summary of ATLAS Run 2 (24.5-139 fb<sup>-1</sup>(13 TeV)) Higgs signal strength measurements [10]. The measurement of  $VH, H \rightarrow WW$  is taken from [11].

Production	Decay channel	Lumi [reference]	Signal strength
ggF	$H \rightarrow ZZ$	139 fb <sup>-1</sup> [10]	$0.94^{+0.11}_{-0.10}$
VBF			$1.25^{+0.50}_{-0.41}$
VH			$1.53^{+1.13}_{-0.92}$
ggF	$H \rightarrow \gamma\gamma$	139 fb <sup>-1</sup> [10]	$1.03 \pm 0.11$
VBF			$1.31^{+0.26}_{-0.23}$
VH			$1.32^{+0.33}_{-0.30}$
$ttH + tH$			$0.90^{+0.27}_{-0.24}$
ggF	$H \rightarrow WW$	36.1 fb <sup>-1</sup> [10]	$1.08^{+0.19}_{-0.18}$
VBF		36.1 fb <sup>-1</sup> [10]	$0.60^{+0.36}_{-0.34}$
VH		36.1 fb <sup>-1</sup> [11]	$2.5^{+0.9}_{-0.8}$
VBF	$H \rightarrow bb$	24.5-30.6 fb <sup>-1</sup> [10]	$3.03^{+1.67}_{-1.62}$
VH		139 fb <sup>-1</sup> [10]	$1.02^{+0.18}_{-0.17}$
$ttH + tH$		36.1 fb <sup>-1</sup> [10]	$0.79^{+0.60}_{-0.59}$
ggF	$H \rightarrow \tau\tau$	36.1 fb <sup>-1</sup> [10]	$1.02^{+0.60}_{-0.55}$
VBF			$1.15^{+0.57}_{-0.53}$
$ttH + tH$			$1.20^{+1.07}_{-0.93}$
$ttH + tH$	$H \rightarrow VV$	36.1 fb <sup>-1</sup> [10]	$1.72^{+0.56}_{-0.53}$

the fermionic degrees of freedom in the global symmetry structure  $G$ . As an example, in the minimal composite Higgs models, based on  $SO(5)/SO(4)$  coset group,  $\Sigma$  will transform as 5-plet of  $SO(5)$  which could form a  $SO(5)$  invariant either with two 5-plets or pair of 5 and 10-plets.

More general CHMs lead to very different patterns of breaking and types of embeddings for the fermion content of the model. Yes, despite spanning many model building options, it was noted in Ref. [35] that the Yukawa couplings usually fall into two choices,

$$\kappa_F^A = \sqrt{1 - \xi} \approx 1 - \frac{1}{2}\xi, \quad (4)$$

$$\kappa_F^B = \frac{1 - 2\xi}{\sqrt{1 - \xi}} \approx 1 - \frac{3}{2}\xi. \quad (5)$$

For example, the models based on coset groups  $SO(5)/SO(4)$  [7, 36],  $SO(6)/SO(4) \times SO(2)$  [37–39],  $SU(5)/SU(4)$  [40], and  $SO(8)/SO(7)$  [41, 42] have fermions-Higgs couplings modified by  $\kappa_F^A$ . On the other hand,  $\kappa_F^B$ -type couplings could exist in  $SO(5)/SO(4)$  [36, 43–45],  $SU(4)/Sp(4)$  [46],  $SU(5)/SO(5)$  [47], and  $SO(6)/SO(4) \times SO(2)$  [37–39] group-based models. In all these models, the Higgs doublet lies within the unbroken subgroup, but in some of those, there could be an extra singlet or Higgs doublet.

A composite Higgs, with nonstandard couplings to massive fermions and bosons, would also exhibit nonstandard

loop-level couplings to gluons and photons ( $\kappa_{g,\gamma}$ ) [9, 48].

$$\begin{aligned} \kappa_g^2 &= 1.06\kappa_t^2 + 0.01\kappa_b^2 - 0.07\kappa_b\kappa_t, \\ \kappa_\gamma^2 &= 1.59\kappa_V^2 + 0.07\kappa_t^2 - 0.66\kappa_V\kappa_t, \end{aligned} \quad (6)$$

as well as deviations on the Higgs width ( $\kappa_H$ )

$$\kappa_H^2 \approx 0.57\kappa_b^2 + 0.25\kappa_V^2 + 0.09\kappa_g^2. \quad (7)$$

Note that  $\kappa_t$  and  $\kappa_b$  do not have to be equal (see Equations (4) and (5)) depending on how fermions are embedded within the global symmetry group.

Putting all this together, we are ready to compare measurements of the Higgs properties with expectations from a nonlinear realisation of EWSB via a composite Higgs. The experimental inputs, described in Tables 2 and 3, are Higgs signal strengths for different production and decay channels. We compare these measurements with theoretical predictions of the signal strength as a function of the  $\kappa$  modifiers  $\kappa_f$ ,  $\kappa_V$ ,  $\kappa_g$ ,  $\kappa_\gamma$ , and  $\kappa_H$ . For example, for the gluon fusion  $g gH$  ( $H \rightarrow \gamma\gamma$ ) channel, it adopts the form:  $\mu^{CH} = \kappa_g^2 \kappa_\gamma^2 / \kappa_H^2$ . Note that all  $\kappa$ 's are a function of a single parameter model,  $f$ , as shown in Equations (3)–(5).

To compare the CHM predictions with Higgs signal strength measurements from CMS and ATLAS experiments, we evaluate the  $\chi^2$  statistic test

$$\chi^2(f) = \sum_i^{\text{Run1, Run2}} \left( \frac{\mu_i(\kappa(f))^{CH} - \mu_i^{\text{Exp}}}{\Delta\mu_i} \right)^2. \quad (8)$$

Here,  $\mu(\kappa(f))^{CH}$ ,  $\mu^{\text{Exp}}$ , and  $\Delta\mu$  denote the model prediction of the signal strength, experimental measurement, and error for the experimental measurement, respectively. The index  $i$  runs over all the measurements from Run 1 and Run 2. Note that the correlations among the different experimental measurements are not considered as they are subdominant with respect to the model uncertainties introduced by the choices of  $\kappa_F$ .

In this section, we only focus on nonlinear effects; hence, the rates  $\mu(\kappa(f))^{CH}$  are sensitive to one parameter, the  $\xi = v^2/f^2$  ratio, and choices for the fermion couplings from Equations (4) and (5). In Figure 2, we show the  $\chi^2$  fit of different choices for  $\kappa_F$  to the combined LHC Run 1 and Run 2 data. Run 1 data is taken from the combined CMS and ATLAS analysis [9]. For Run 2 data, individual measurements from CMS [12–16] (see Table 2) and ATLAS [10, 11] (see Table 3) are considered. For  $H \rightarrow b\bar{b}$  decay channel, both CMS and ATLAS have combined Run 1 and Run 2 data measurements so we have not considered the single Run 1 measurements.

In Figure 2, we show the 1- and 2-sigma limits on  $\Delta\chi^2 = \chi^2 - \chi_{\min}^2$  in green and yellow, respectively. The  $\chi_{\min}^2$  value is approx 46 with 59 observables, which leads to  $\chi^2/n_{\text{dof}}$  approximately 0.78. The values of  $\Delta\chi^2$  depend on whether the top, bottom, and tau  $\kappa$  modifiers are of type A or B.



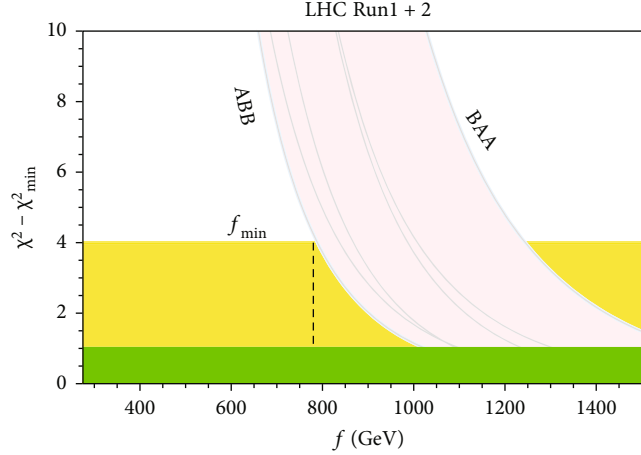


FIGURE 2:  $\Delta\chi^2 = \chi^2(f) - \chi^2_{\min}$  for the combination of Run 1 and 2 LHC data (signal strength measurements). The different grey lines correspond to different choices of fermion couplings  $\kappa_F^{A,B}$  for  $(\kappa_t, \kappa_b, \kappa_\tau)$ . The vertical line is the lowest allowed value (95% C.L.) of the compositeness scale ( $f_{\min}$ ) within a model where fermion couplings are of the ABB type, i.e., top quark have  $\kappa_F^A$ , bottom and tau have  $\kappa_F^B$  factors in the Higgs couplings. Label BAA type represents the case when top quark has a  $\kappa_F^B$  modifier, whereas the bottom and tau have  $\kappa_F^A$ . Green and yellow are the  $1\sigma$  and  $2\sigma$  regions, respectively.

Following Ref. [35], we plot all the lines with all combinations. We also denote which combination is less constrained, corresponding to  $\kappa_t = \kappa_F^A$ ,  $\kappa_b = \kappa_F^B$ , and  $\kappa_\tau = \kappa_F^B$ , and denoted by the symbol ABB. We also denote which combination of coupling choices is constrained more strongly by LHC data, BAA in the same notation. Note that the less constrained option, ABB, corresponds to a smaller deviation of top couplings than bottom and tau, see Equations (4) and (5).

Comparing with Ref. [35], we obtain a stronger lower bound on the scale of compositeness of  $f_{\min} = 780$  GeV ( $f_{\min}$  is a minimum scale at which the considered fermion coupling combination is compatible with the data at  $2\sigma$  level.). The different curves highlight the fact that there is roughly 500 GeV variation in the  $f_{\min}$  scale, reaching  $f_{\min} \sim 1.3$  TeV for the most tightly bound scenario.

**2.2. CHM Pattern II: Extended Higgs Sectors.** When the group  $G$  breaks down to  $H$ , light degrees of freedom are generated. Only in specific configurations one would expect exactly four Goldstones, to match the SM needs. Hence, generic composite Higgs scenarios would typically exhibit a pattern of extended Higgs sectors, with more light scalars involved in EWSB. In the simplest of such extensions, one would consider an additional singlet, see, e.g., [49], which could mix with the SM-like Higgs doublet. The next simplest iteration would introduce new doublets, as is the case in, e.g., the coset group  $SO(6)/SO(4) \times SO(2)$  [39], where the light degrees of freedom organise as a two Higgs doublet model (2HDMs) [50].

Doublets and singlets are not the only model-building possibilities which composite Higgs models offer, e.g., on the  $SU(6)/SO(6)$  coset, one has two Higgs doublets but also a custodial bitriplet [51]. Generically speaking, a composite Higgs scenario leading to one single doublet at low energies

is minimal but not typical, and one should consider the effect of more scalars involved in EWSB.

Moreover, this pattern opens new, interesting possibilities for model building beyond EWSB. These extra singlet or doublet pseudo-Goldstones could play a role in Inflation [52, 53] or act as dark matter candidates [51]. In composite Higgs scenarios, these new scalars could help on enhancing the strength of the electroweak phase transition [54] by introducing new sources of CP violation and more interesting phase diagram structures, and even play some role in the QCD CP problem [55].

In this section, we explore what the Run 2 LHC data can tell us about these extensions. We will discuss the modification of the gauge boson and fermions couplings to the SM-like Higgs boson when the additional scalars mix with the SM-like Higgs. Their effect could also be felt at loop level, even in the absence of a mixing, but these contributions would be suppressed by loop factors respect to mixing. Both possibilities, mixing and loop effects, were computed and explored in Ref. [56], and here, we make use of these theoretical calculations and update the limits in the context of CHMs and the possible interplay between mixing and nonlinearities.

**2.2.1. Singlet Scalar.** The presence of an extra singlet modifies the  $\kappa_{F/V}$  by a factor of  $\cos \theta_S$ , where  $\theta_S$  denotes the mixing angle between the neutral scalar  $h$  and the extra singlet scalar field. This effect is simply due to linear mixing terms when both the singlet and the SM-like Higgs get their VEVs. Nonlinearities due to the origin of the SM-like Higgs as a composite Higgs would still be present, in exactly the same way we discussed in Section 2.1 (One could consider situations where the additional singlets or doublets do participate directly in the mechanism for EWSB, as shown in the seesaw composite Higgs [57], where this assumption would fail).

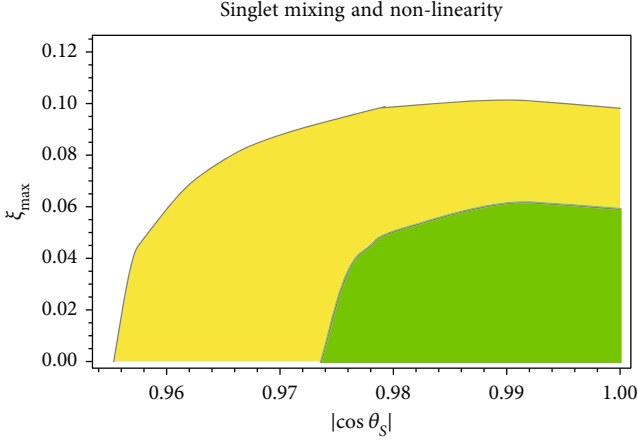


FIGURE 3: The bound on the  $\xi_{\max}$  as a function of  $\cos \theta_S$  in case of singlet mixing scenario for the ABB type model.

TABLE 4: The  $\kappa_V$  and  $\kappa_F$  expressions in two Higgs doublet models. Here,  $s_x/c_x/t_x = \sin x/\cos x/\tan x$ .

Model	$\kappa_V$	$\kappa_F$
Type-I	$s_{\beta-\alpha}$	$\kappa_u = \kappa_d = \kappa_\ell = (c_{\beta-\alpha}/t_\beta) + s_{\beta-\alpha}$
Type-II	$s_{\beta-\alpha}$	$\kappa_u = (c_{\beta-\alpha}/t_\beta) + s_{\beta-\alpha}$ $\kappa_d = \kappa_\ell = s_{\beta-\alpha} - t_\beta c_{\beta-\alpha}$
$\ell$ -specific	$s_{\beta-\alpha}$	$\kappa_u = \kappa_d = (c_{\beta-\alpha}/t_\beta) + s_{\beta-\alpha}$ $\kappa_\ell = s_{\beta-\alpha} - t_\beta c_{\beta-\alpha}$
Flipped	$s_{\beta-\alpha}$	$\kappa_u = \kappa_\ell = (c_{\beta-\alpha}/t_\beta) + s_{\beta-\alpha}$ $\kappa_d = s_{\beta-\alpha} - t_\beta c_{\beta-\alpha}$

Therefore, the Higgs couplings to vector bosons would be doubly modified as

$$\kappa_V = \cos \theta_S \sqrt{1 - \xi} \approx 1 - \frac{1}{2}\xi - \frac{1}{2}\theta_S^2, \quad (9)$$

where we have expanded for small values of nonlinearities and mixing to show how these two effects work in the same direction, i.e., to reduce the coupling value from the SM expectation.

The nonlinear part of the modification of the fermion couplings depends on the fermion embedding in representations of the global symmetry. As discussed before, we find two main choices for  $\kappa_F$ , namely,

$$\kappa_F^A = \cos \theta_S \sqrt{1 - \xi} \approx 1 - \frac{1}{2}\xi - \frac{1}{2}\theta_S^2 \quad (10)$$

or

$$\kappa_F^B = \cos \theta_S \frac{1 - 2\xi}{\sqrt{1 - \xi}} \approx 1 - \frac{3}{2}\xi - \frac{1}{2}\theta_S^2, \quad (11)$$

where again we expand for small modifications  $\xi$  and  $\theta_S$  to

show explicitly the cooperative effort of both effects to lower the coupling.

We perform the fit to the Higgs data as in Section 2.1 but now including the effect of mixing,  $\chi^2(f, \theta_S)$ . As shown in Figure 2, we vary options for the fermion couplings and find the  $f_{\min}$ . We perform this fit for different values of the mixing angle, always finding the minimum  $f$  corresponding to a set of options for  $\kappa_F$ . The result of this procedure is shown in Figure 3, where we plot  $\xi_{\max} = v^2/f_{\min}^2$  scale as a function of the singlet mixing. On the right side of the plot, we see the effect of small mixing, where we recover the result from the previous section. As we move towards the left in the plot, the mixing becomes more important and at some point  $\xi_{\max} \rightarrow 0$ , we obtain the pure mixing limit of  $|\cos \theta_S| \approx 0.96$ .

Note that the mixing angle is determined by singlet mass ( $m_S$ ), singlet vev ( $v_S$ ), and quadratic coupling of light Higgs doublet and singlet scalar ( $\lambda$ ), as given below

$$\cos \theta_S = \cos \left( \frac{v^2}{(m_S^{\text{eff}})^2} \right); m_S^{\text{eff}} = \frac{m_S}{\sqrt{\lambda(v_S/v)}}, \quad (12)$$

where  $v = 246$  GeV. Therefore, the limit  $|\cos \theta_S| \approx 0.96$  would be equivalent to  $m_S^{\text{eff}} \parallel 450$  GeV.

In between these two asymptotic limits, the constraints on the scales  $f$  and  $m_S^{\text{eff}}$  become stronger, as both mixing and nonlinearities work together to reduce the Higgs couplings.

**2.2.2. Two Higgs Doublet Models (2HDM).** As discussed in the previous section, the mixing effect due the additional Higgs in a composite Higgs model does not typically couple with the nonlinear effects at leading order. Hence, in composite two Higgs doublet models, the vector and fermion couplings to the Higgs,  $\kappa_{V/f}$ , would still adopt this factorisable form  $\kappa_{V/F}^{2\text{HDM}} \times \kappa_{V/F}^{\text{CH}}$ , where  $\kappa_{V/F}^{\text{CH}}$  has been discussed in Section 2.1 and  $\kappa_{V/F}^{2\text{HDM}}$  correspond to the modifications of the SM-like Higgs couplings in 2HDM models.

The explicit form of  $\kappa_{V/F}^{2\text{HDM}}$  is given in Table 4 for various types of 2HDM models. In these scenarios, vector and fermion modifiers are determined by two parameters, the ratio of symmetry breaking VEVs of Higgs doublets ( $\tan \beta$ ), and neutral Higgs mixing angle ( $\alpha$ ).

In our analysis, we only consider the main scenarios, Type I and Type II. The  $\chi^2_{2\text{CHM}}$  statistical test for a composite Higgs with possible mixing with another doublet becomes a function of three parameters:  $f$ ,  $\cos(\beta - \alpha)$ , and  $\tan \beta$ .

First, we discuss the information that Run 2 LHC data provides on type I and II 2HDMs, without considering the nonlinear effects. This information is shown in Figure 4, where the coloured regions green, yellow, and red represent 68%, 95%, and 98% C.L. limits in the  $\cos(\beta - \alpha) - \tan \beta$  plane, respectively. As expected, the SM-like Higgs prefers a region with  $\cos \beta - \alpha \approx 0$ , the alignment limit [58].

The alignment limit can be understood in terms of the potential parameters in the 2HDM, couplings between the two doublets  $\tilde{\lambda}_i$  and masses  $\tilde{\mu}_{1,2}$ , see Ref. [56] for more details.

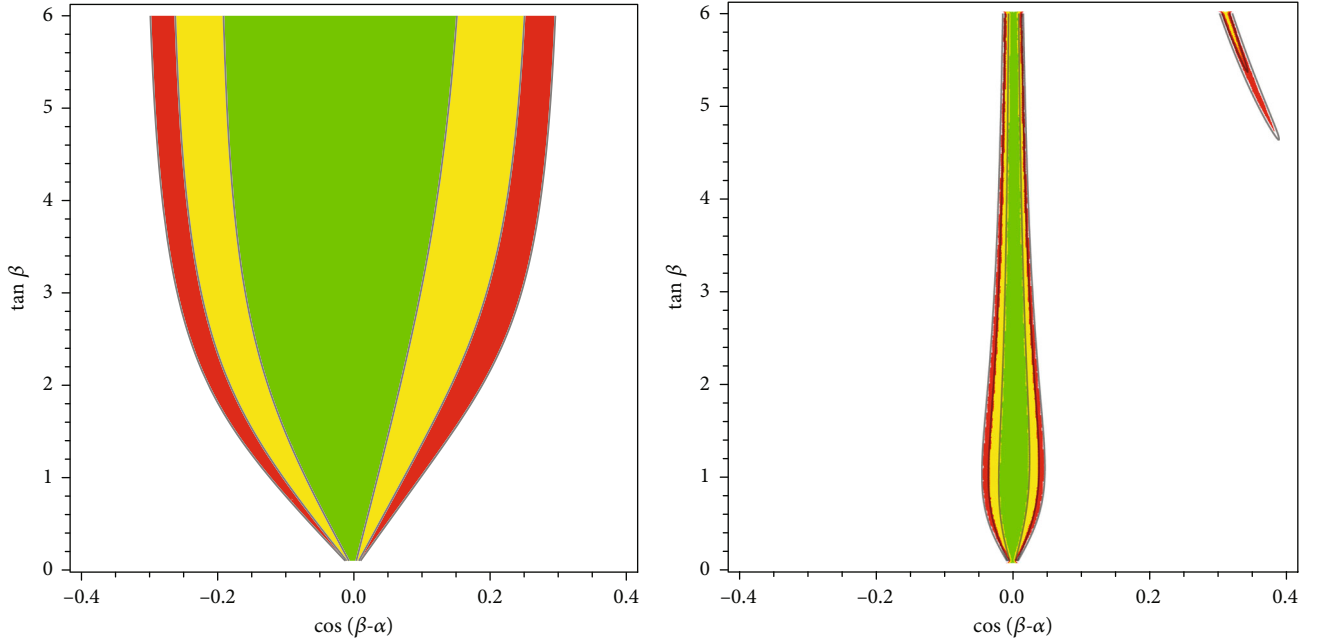


FIGURE 4: The 68% (green), 95% (yellow), and 98% (red) C.L. limits in the  $\cos(\beta - \alpha) - \tan \beta$  plane for 2HDM type I (a) and type II (b) with  $\xi = 0$ .

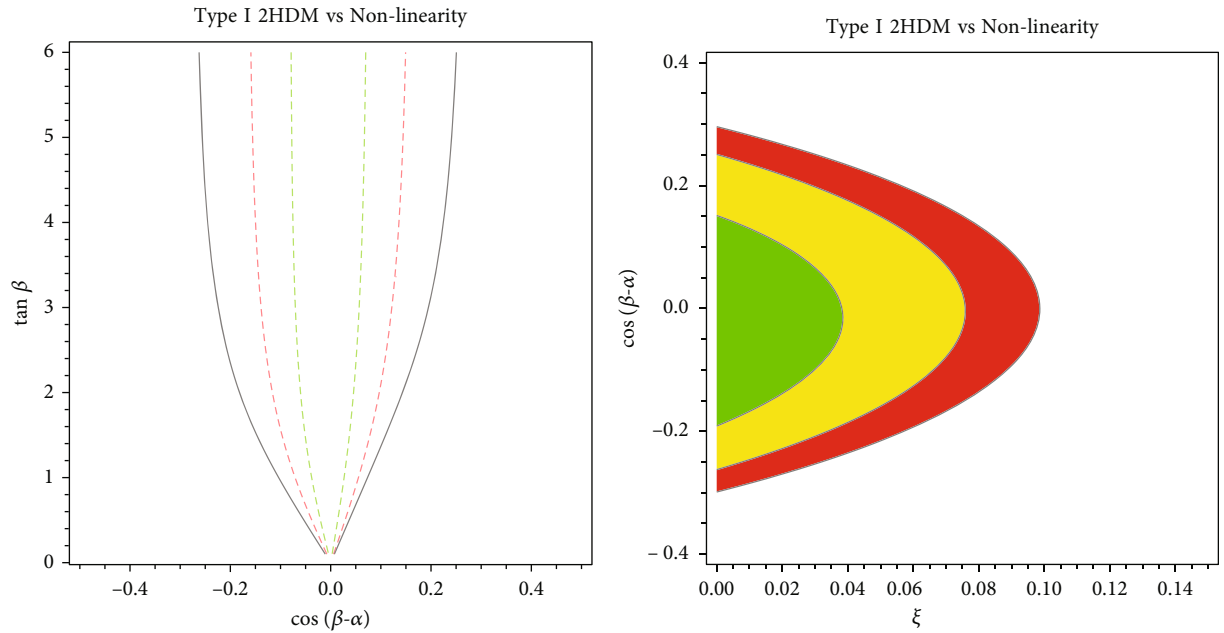


FIGURE 5: Type I 2HDM results. (a) The 95% C.L. limit including nonlinear effects. The black, red, and green lines correspond to choices of the parameter  $\xi = 0, 0.05$ , and  $0.07$ , respectively. (b) The 68% (green), 95% (yellow), and 98% (red) C.L. limits in the  $\xi - \cos(\beta - \alpha)$  plane for  $\tan \beta = 6$ .

In terms of these parameters, the deviation from the alignment limit can be parametrised as  $\cos \beta - \alpha \sim \lambda_6 v^2 / \tilde{\mu}_2^2$ .

Next, we introduce the additional nonlinear effects in Figure 5(a), where we show how the 95% C.L. regions are modified with nonlinear effects. The nonlinear effects, as in the case of the singlet, add up to the doublet mixing. Larger

nonlinearities restrict further the parameter space of 2HDMs.

Finally, as the  $\tan \beta$  dependence is rather mild for  $\tan \beta \parallel 2$ , we fix the value of  $\tan \beta = 6$  to explore the interplay between  $\cos \beta - \alpha$  and  $\xi$ . In Figure 5(b), we plot the one-, two-, and three- $\sigma$  contours in this plane. In the alignment

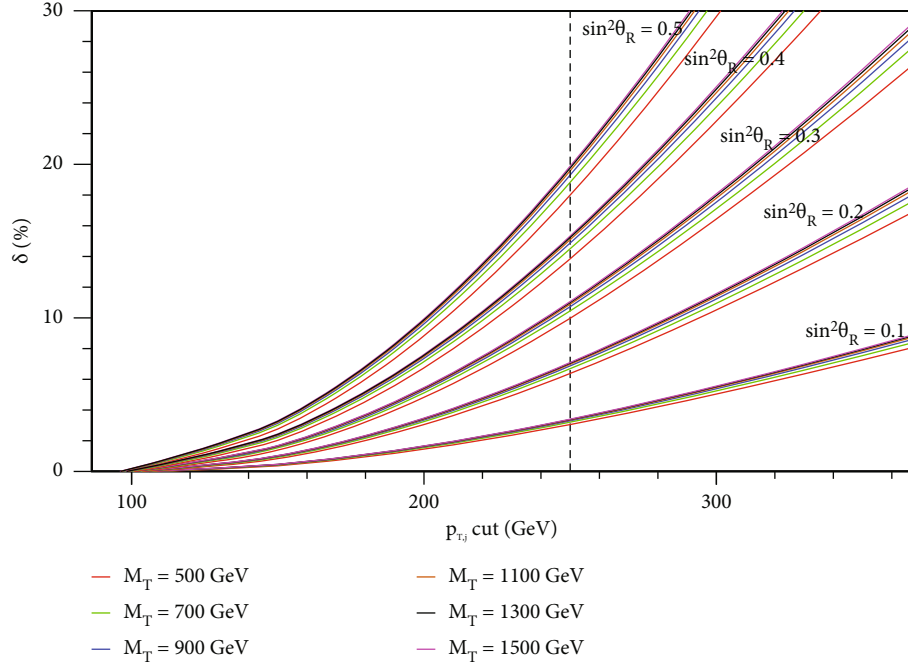


FIGURE 6: Percentage enhancement in the Higgs+jet cross-section by the top-partner contribution as a function of  $p_T^{\text{cut}}$  for different values of mixing angle and  $M_T$ .

limit,  $\cos \beta - \alpha \approx 0$ , we recover the pure nonlinear limit  $\xi \approx 0.08$  at 95% C.L. As we move from the alignment limit and allow a larger amount of doublet mixing, the limit on  $\xi$  becomes milder, leading to a stronger bound on the compositeness scale  $f$ . On the left side of the plot where  $\xi \rightarrow 0$ , we find the limit on non-decoupling effects  $\cos \beta - \alpha \approx 0.25$  at 95% C.L., which would correspond to the scale for the second doublet  $\tilde{\mu}_2 \sim 500$  GeV for  $\lambda_6 \sim O(1)$ .

**2.3. CHM Pattern III: Extended Fermionic Sector.** We finish this section on patterns, analysing a typical building block in composite Higgs scenarios: the presence of new fermionic degrees of freedom, not too far from the electroweak scale. These fermionic degrees of freedom are usually coming along as top partners, new vector-like fermions which mix with the SM top quark and modify its couplings with the Higgs.

We first focus on the mixing and present results for the  $SU(2)_L$ -singlet top-partner scenario  $T_{L,R}^0$ . We calculate the indirect bound on these states from measurements on the differential distributions of the boosted Higgs in association with an energetic jet. The methodology used here was developed in Ref. [59] and further expanded in Refs. [60, 61]. We will then evaluate other sources of experimental constraints, including direct searches for the new state.

To describe the effect of the top-partner in the Higgs behaviour, we need to specify the mixing parameters between the top-partner and the SM top quark. For the singlet case, the mass matrix of the SM top quark and Dirac fer-

mion top-partner  $T = (T_L, T_R)$  can be written as

$$(\bar{t}_L \bar{T}_L) \begin{pmatrix} \frac{y_t h}{\sqrt{2}} & \Delta & 0 \\ 0 & M & 0 \end{pmatrix} (t_R T_R), \quad (13)$$

where  $\Delta$  describes the mixing between  $t$  and  $T$  and  $M$  is the Dirac mass of the top partner. After diagonalising this matrix by a biunitary transformation, we can calculate the mass eigenstates  $M_T$  and  $m_t$  and the mixing angle

$$\theta_R = \frac{1}{2} \sin^{-1} \left( \frac{2m_t M_T \Delta}{(M_T^2 - m_t^2) M} \right). \quad (14)$$

Note that  $\theta_R$  and  $\theta_L$  are related in a simple way,

$$\tan \theta_L = \frac{M_T}{m_t} \tan \theta_R. \quad (15)$$

**2.3.1. Top-Partner Indirect Searches.** Contrary to the previous sections, total Higgs rates and their respective limits on vector and fermion couplings  $\kappa_{V/F}$  would not be sensitive to the presence of the top-partner. On the other hand, high- $p_T$  probes would access the top-partner mixing and mass scale indirectly [59, 60].

To analyse the effect of  $T$  in the Higgs production in association with radiation, it is useful to define a quantity which depends on  $M_T$  and  $\theta_R$  based on semidifferential



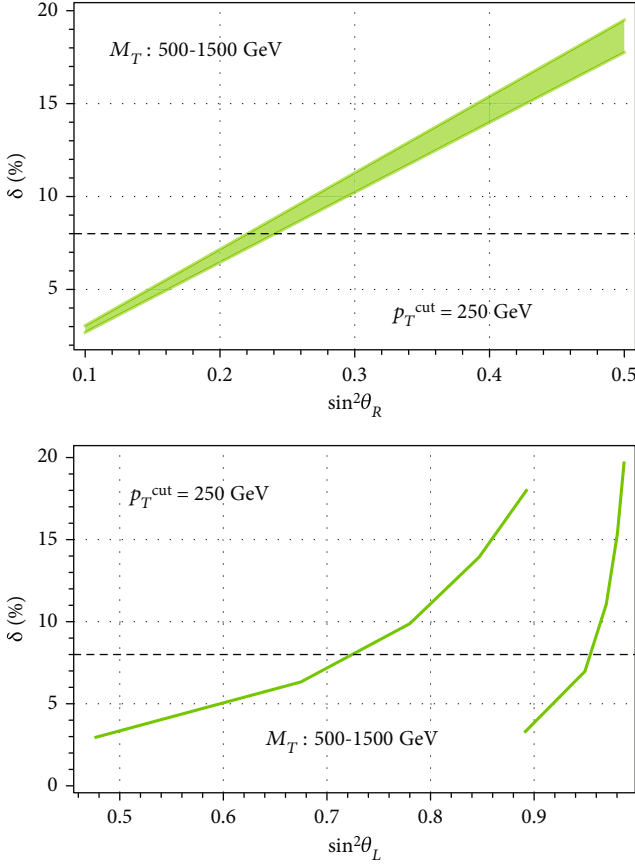


FIGURE 7: Percentage enhancement in the Higgs+jet cross-section by the top-partner contribution ( $\delta$ ) as a function of the top-partner mixing angle for  $p_T^{\text{cut}} = 250$  GeV. The horizontal hashed line corresponds to the experimental bound [17], and the band width to the variation in  $M_T \in [500, 1500]$  GeV.

measurements,

$$\sigma(p_T > p_T^{\text{cut}}) = \int_{p_T^{\text{cut}}}^{\infty} dp_T \frac{d\sigma}{dp_T}. \quad (16)$$

In particular, we define a quantity based on these differential measurements,

$$\delta(p_T^{\text{cut}}, M_T, \sin \theta_R) = \frac{\sigma_{t+T}(p_T^{\text{cut}}, M_T, \sin \theta_R) - \sigma_t(p_T^{\text{cut}})}{\sigma_t(p_T^{\text{cut}})}, \quad (17)$$

which exhibits good properties from the point of view of systematic and statistical fluctuations, see Ref. [59] for more details.

With this observable as an indirect probe for fermionic top-partners, we calculated  $\sigma_t$  and  $\sigma_{t+T}$  for  $\sqrt{s} = 13$  TeV by varying  $M_T$  and  $\sin \theta_R^2$ . The results can be seen in Figure 6, where we plot the relative change in the Higgs+jet cross-section as a function of  $p_T^{\text{cut}}$  for different combinations of the mixing angle and  $M_T$ . For this plot,  $M_T$  is varied from 500 GeV to 1500 GeV, and one can see that  $\delta$  has a weak

dependence on  $M_T$ . We can then use the experimental measurements in this channel to put a bound on the mixing angle. In particular, we used the ATLAS Higgs differential cross-section analysis [17], which reports an 8% deviation at 95% C.L. in the 250-350 GeV (diphoton)  $p_T$  bin from the SM cross-section. We can then look back at our Figure 6 and note the variation of  $\delta$  as a function of  $\sin \theta_R$  for  $p_T^{\text{cut}} = 250$  GeV.

In Figure 7, we show the variation of  $\delta$  as a function of  $\sin \theta_R$  for a fixed  $p_T^{\text{cut}} = 250$  GeV. The green band corresponds to varying  $M_T$  from 500 GeV to 1500 GeV. The 8% limit is noted with a hashed black line, which allows us to set a limit on  $\sin^2 \theta_R 0.25$ . Using Equation (15), the corresponding limit in terms of the parameter  $\sin \theta_L$  is also obtained, see the lower panel of Figure 7.

Another source of constraints from a singlet VLQ top-partner would come from a SM effective field theory (SMEFT) global analysis of Run 2 LHC and LEP measurements. The singlet top-partner would produce a SMEFT pattern characterised by relations among some SMEFT operators, whereas all the other operators would be zero at tree level, see Ref. [62] for a dictionary between many extensions of the SM and their SMEFT matching, see also the discussion in Ref. [63] on the top-partners and the SMEFT framework. Using this dictionary and a global SMEFT analysis, in Ref. [64], the parameters of the singlet top-partner were bound to  $\sin \theta_L^2 0.05$  for  $M_T \approx 1$  TeV.

**2.3.2. Top-Partner Direct Searches.** Boosted Higgs measurements provide one handle on top-partners. The LHC New Physics search programme includes very mature analyses looking for single and pair production of vector-like Quarks (VLQ). Pair production of VLQs is a dominantly strong interaction process, whereas single production relies on electroweak couplings.

A singlet up-type VLQ (T) is excluded up to 1.31 TeV by the ATLAS  $\sqrt{s} = 13$  TeV ( $36.1 \text{ fb}^{-1}$ ) search for pair produced VLQs [65] after considering all decay modes. This limit is a combined limit from several searches for the pair production of VLQs.

From the CMS side, there are separate limits from each analysis of pair production of VLQs. The exclusion limit on singlet  $T$  from dilepton final state of VLQs decaying to  $Z$  boson is 1280 GeV [66]. The CMS analysis for all leptonic final states excludes  $M_T$  in the range 1140-1300 GeV corresponding to different branching fractions [67], and the analysis of the  $bW\bar{b}W$  final state excludes singlet  $T$  up to 1295 GeV [68]. The analysis targeting fully hadronic final states provides a bound up to 1.3 TeV for a specific combination of the branching fractions of VLQs [69].

The single VLQ production process is mediated by its coupling with SM particles; hence, it provides a bound on the mixing as a function of the mass of VLQs [18–20]. Both the production cross-section and decay branching ratios are sensitive to mixing effects. The communication of the single-production results is a bit more cumbersome than for double production. In some analyses, this mixing is directly parametrised by the mixing angle ( $\sin \theta_{L,R}$ ) and sometimes by

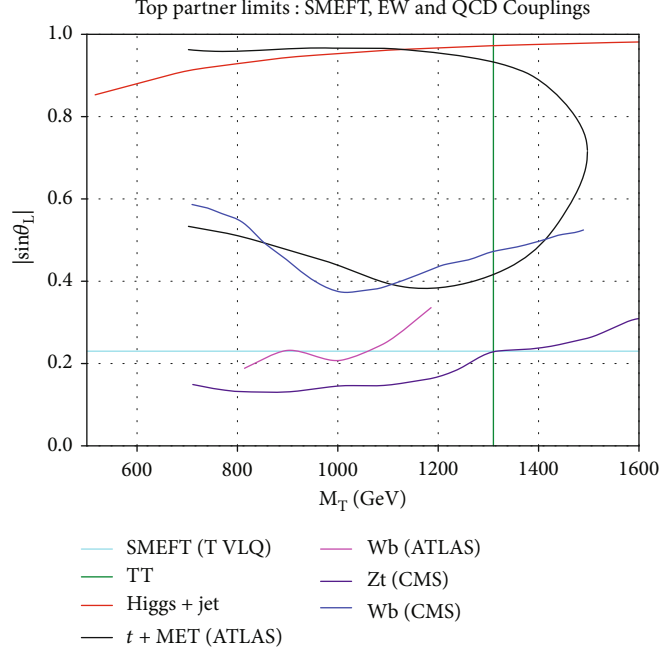


FIGURE 8: Direct searches bounds on singlet top-partners from single and double production of VLQs and indirect bounds from the Higgs +jet final state. Blue, orange, green, and violet curves correspond to the ATLAS single VLQ bound from  $Wb$  channel [18], ATLAS bound from top+MET final state [19], CMS  $Wb$  final state [20], and CMS  $Zt$  final state [21], respectively. The vertical line corresponds to the ATLAS pair production bound [65]. The SMEFT bound is taken from Ref. [64], and the red line indicates the limit from Higgs+jet differential distributions discussed in Section 2.3.1.

the coupling  $c^{bw}$  where  $c_{L/R}^{bw} = \sqrt{2} |\sin \theta_{L/R}|$  [70] is just a rescaling of the mixing angle. ATLAS analysis cross-section limits are interpreted in terms of either  $|\sin \theta_L|$ , or both  $C_W^2 = (c_L^{bw})^2 + (c_R^{bw})^2$  and  $|\sin \theta_L|$ . Note that both the angles  $\sin \theta_L$  and  $\sin \theta_R$  are related by Equation (16).

On the other hand, CMS exclusion limits on production cross-section times branching fraction are provided only as a function of  $m_{VLQ}$ . Additionally, the theoretical cross-section is provided for the fixed value of BR and  $c^{bw} = 0.5$ . We use this additional information to calculate the approximate bound on  $c^{bw}$  as a function of  $m_{VLQ}$ .

We translate CMS bound in terms of mixing angle  $|\sin \theta_L|$  by parametrizing the production cross-section as  $\sigma(T) \times \text{BR}(T \rightarrow bW) = \tilde{\sigma}(T) c^{bw^2} \times \text{BR}(T \rightarrow bW)$ , where  $\tilde{\sigma}(T)$  is calculated from the theoretical cross-section with fixed  $c^{bw}$ . Then, using the bound on cross-section (including BR), we calculate the limit on  $c^{bw}$  which we further translate to  $|\sin \theta_L|$  using the relation  $c_{L/R}^{bw} = \sqrt{2} |\sin \theta_{L/R}|$ . Note that we have not considered the effect of  $C_W$  variation on the width of  $T$ . We also consider other decay channels of the singlet vector-like top to  $ht$  and  $Zt$ . Note that CMS analyses for  $Wb$  [20] and  $Zt$  [21] final states do assume 100% branching ratio, and the ATLAS collaboration has considered  $Wb$  and top+MET final states [19] assuming  $\text{BR}(T \rightarrow Zt) = 0.25$  from the singlet model.

In Figure 8, we show all these direct and indirect limits together in the plane of top-partner mass versus mixing angle. Double production of VLQs (dark-green vertical line) sets a limit on the mass  $M_T \approx 1.3$  TeV. The SMEFT limit

(light blue horizontal line) is very strong and independent of the top-partner mass as long as  $M_T v$ . The current sensitivity of the other indirect probe for top-partners, the  $H$  +jet channel, is below the SMEFT fit, although it is worth noticing that our  $H$ +jet analysis is not at the same level of sophistication as the SMEFT's [64]. Note that for the ATLAS top+MET analysis (black line) the  $|\sin \theta_L|$  values covered by the closed contour are excluded.

### 3. Conclusions

In this work, we have studied the impact of the LHC Run 2 measurements on general composite Higgs scenarios.

The dataset we used includes Higgs signal strength measurements from CMS and ATLAS, differential properties of boosted Higgs production, several searches for single and double production of vector-like quarks and a specific result from a global fit to SMEFT properties obtained in Ref. [64].

We have described the most significant deviations expected from composite Higgs scenarios, going from the simplest effects, nonlinear couplings, to the most complex interplay between direct and indirect searches for additional fermionic degrees of freedom.

We have shown how in general composite Higgs scenarios one should expect simultaneous effects from more than one source. Typically, the composite nature of the Higgs is tied to the non-linear realisation of EWSB and the scale of compositeness  $f$ . But generic composite Higgs scenarios exhibit a richer phenomenology, in particular new light scalars or fermions are also typical predictions of these scenarios.

These new degrees of freedom, if close enough to the electroweak scale, will also modify the Higgs couplings. For example, mixing of additional scalars participating in EWSB will add to nonlinearities to reduce even further the couplings of the Higgs to massive particles, leading then to even stronger limits on the scale of compositeness  $f$ . Note that this scale is tied to the mass of new vector resonances like  $W'$  and  $Z'$  and to the degree of tuning of Higgs potential. The Run 2 LHC data has pushed this scale into the TeV range, and we have shown that more complex scenarios would push this tuning even further. Hence, Run 3 and future LHC runs should have a good handle at natural composite Higgs scenarios.

Finally, we would like to mention that the same scale  $f$  studied in this work could be linked to the the phenomenology of additional pseudo-Goldstone degrees of freedom which could appear in generic CHMs. The study of the correlations between the Higgs phenomenology presented here and the axion-like particles (ALPs) would be very interesting but goes beyond the scope of the paper.

## Data Availability

This paper does not use data sources; it simply uses public cited results on limits from experimental searches. Therefore, no datasets have been generated during this study.

## Disclosure

The manuscript is uploaded on arxiv with the number (arXiv:2102.13429 [hep-ph]) [71].

## Conflicts of Interest

The authors declare that they have no conflicts of interest.

## Acknowledgments

This work of V.S. is supported by the Science Technology and Facilities Council (STFC) under grant number ST/P000819/1. We want to thank Stephan Huber and Jack Setford for many fruitful discussions during the early stages of this work. We thank Andrea Banfi for the help regarding running the Higgs+jet process in his code implementation.

## References

- [1] ATLAS Collaboration, "Observation of a new particle in the search for the standard model Higgs boson with the ATLAS detector at the LHC," *Physics Letters B*, vol. 716, no. 1, pp. 1–29.
- [2] CMS Collaboration, "Observation of a new boson at a mass of 125 GeV with the CMS experiment at the LHC," *Physics Letters B*, vol. 716, no. 1, pp. 30–61, 2012.
- [3] The ATLAS collaboration, "Measurements of the Higgs boson production and decay rates and constraints on its couplings from a combined ATLAS and CMS analysis of the LHC  $pp$  collision data at  $\sqrt{s} = 7$  and 8 TeV," *Journal of High Energy Physics*, vol. 8, p. 45, 2016.
- [4] D. B. Kaplan, H. Georgi, and S. Dimopoulos, "Composite Higgs scalars," *Physics Letters B*, vol. 136, pp. 187–190, 1984.
- [5] M. J. Dugan, H. Georgi, and D. B. Kaplan, "Anatomy of a composite Higgs model," *Nuclear Physics B*, vol. 254, pp. 299–326, 1985.
- [6] R. Contino, Y. Nomura, and A. Pomarol, "Higgs as a holographic pseudo-Goldstone boson," *Nuclear Physics B*, vol. 671, pp. 148–174, 2003.
- [7] K. Agashe, R. Contino, and A. Pomarol, "The minimal composite Higgs model," *Nuclear Physics B*, vol. 719, no. 1–2, pp. 165–187, 2005.
- [8] E. Furlan, *Phenomenology of composite Higgs models*, Zurich, ETH, 2010.
- [9] The ATLAS collaboration, "Measurements of the Higgs boson production and decay rates and constraints on its couplings from a combined ATLAS and CMS analysis of the LHC  $pp$  collision data at  $\sqrt{s} = 7$  and 8 TeV," *Journal of High Energy Physics*, vol. 1608, article 45, 2016.
- [10] The ATLAS collaboration, "A combination of measurements of Higgs boson production and decay using up to 139 fb<sup>-1</sup> of proton–proton collision data at  $\sqrt{s} = 13$  TeV collected with the ATLAS experiment," <https://cds.cern.ch/record/2725733>.
- [11] ATLAS Collaboration, "Measurement of the production cross section for a Higgs boson in association with a vector boson in the  $H \rightarrow WW^* \rightarrow \ell\nu\ell\nu$  channel in  $pp$  collisions at  $\sqrt{s} = 13$  TeV with the ATLAS detector," <https://arxiv.org/abs/1903.10052>.
- [12] The CMS collaboration, "Combined Higgs boson production and decay measurements with up to 137 fb<sup>-1</sup> of proton–proton collision data at  $\sqrt{s} = 13$  TeV," <https://cds.cern.ch/record/2706103>.
- [13] The CMS Collaboration, "Measurements of Higgs boson properties in the diphoton decay channel at 13 TeV," <https://cds.cern.ch/record/2725142>.
- [14] CMS Collaboration, "Observation of Higgs Boson Decay to Bottom Quarks," *Physical Review Letters*, vol. 121, no. 12, article 121801, 2018.
- [15] CMS, "Higgs boson production in association with top quarks in final states with electrons, muons, and hadronically decaying tau leptons at 13 TeV," <https://cds.cern.ch/record/2725523>.
- [16] CMS, "Measurement of Higgs boson decay to a pair of muons in proton-proton collisions at 13 TeV," <https://cds.cern.ch/record/2725423>.
- [17] The ATLAS collaboration, "Measurements and interpretations of Higgs-boson fiducial cross sections in the diphoton decay channel using 139 fb<sup>-1</sup> of  $pp$  collision data at 13 TeV with the ATLAS detector," <https://cds.cern.ch/record/2682800>.
- [18] ATLAS Collaboration, "Search for single production of vector-like quarks decaying into  $Wb$  in  $pp$  collisions at  $\sqrt{s} = 13$  TeV with the ATLAS detector," <https://arxiv.org/abs/1812.07343>.
- [19] ATLAS Collaboration, "Search for large missing transverse momentum in association with one top-quark in proton-proton collisions at  $\sqrt{s} = 13$  TeV with the ATLAS detector," <https://arxiv.org/abs/1812.09743>.
- [20] CMS Collaboration, "Search for single production of vector-like quarks decaying into a  $b$  quark and a  $W$  boson in proton-proton collisions at  $\sqrt{s} = 13$  TeV," <https://arxiv.org/abs/1701.08328>.
- [21] CMS Collaboration, "Search for single production of a vector-like  $T$  quark decaying to a  $Z$  boson and a top quark in proton–

- proton collisions at  $\sqrt{s} = 13\text{TeV}$ ,” *Physics Letters B*, vol. 781, pp. 574–600, 2018.
- [22] F. Feruglio, “The Chiral approach to the electroweak interactions,” *International Journal of Modern Physics A*, vol. 8, pp. 4937–4972, 1993.
  - [23] B. Grinstein and M. Trott, “Higgs-Higgs bound state due to new physics at a TeV,” *Physical Review D*, vol. 76, article 073002, 2007.
  - [24] D. J. E. Marsh, “Axions and ALPs: a very short introduction,” <https://arxiv.org/abs/1712.03018>.
  - [25] K. Mimasu and V. Sanz, “ALPs at colliders,” *Journal of High Energy Physics*, vol. 2015, article 173, 2015.
  - [26] J. Jaeckel and M. Spannowsky, “Probing MeV to 90 GeV axion-like particles with LEP and LHC,” *Physics Letters B*, vol. 753, pp. 482–487, 2016.
  - [27] M. Bauer, M. Neubert, and A. Thamm, “Collider probes of axion-like particles,” *Journal of high energy physics*, vol. 2017, article 44, 2017.
  - [28] I. Brivio, M. B. Gavela, L. Merlo et al., “ALPs effective field theory and collider signatures,” *The European Physical Journal C*, vol. 77, article 572, 2017.
  - [29] M. B. Gavela, J. M. No, V. Sanz, and J. F. de Trocóniz, “Non-resonant searches for axionlike particles at the LHC,” *Physical Review Letters*, vol. 124, article 051802, 2020.
  - [30] J. Ebadi, S. Khatibi, and M. Mohammadi Najafabadi, “New probes for axionlike particles at hadron colliders,” *Physical Review D*, vol. 100, article 015016, 2019.
  - [31] C. G. Callan Jr., S. R. Coleman, J. Wess, and B. Zumino, “Structure of Phenomenological Lagrangians. II,” *Physical Review*, vol. 177, article 2247, 1969.
  - [32] R. Contino, “The Higgs as a composite Nambu-Goldstone boson,” *Physics of the Large and the Small*, pp. 235–306, 2011.
  - [33] I. Brivio, T. Corbett, O. J. P. Éboli et al., “Disentangling a dynamical Higgs,” *Journal of High Energy Physics*, vol. 2014, article 24, 2014.
  - [34] R. Contino, T. Kramer, M. Son, and R. Sundrum, “Warped/composite phenomenology simplified,” *Journal of High Energy Physics*, no. article 74, 2007.
  - [35] V. Sanz and J. Setford, “Composite Higgs models after Run 2,” *Advances in High Energy Physics*, vol. 2018, Article ID 7168480, 2018.
  - [36] M. Carena, L. Da Rold, and E. Pontón, “Minimal composite Higgs models at the LHC,” *Journal of High Energy Physics*, vol. 1406, article 159, 2014.
  - [37] S. De Curtis, S. Moretti, K. Yagyu, and E. Yildirim, “LHC phenomenology of composite 2-Higgs doublet models,” *The European Physical Journal C*, vol. 77, no. 8, p. 513, 2017.
  - [38] S. De Curtis, S. Moretti, K. Yagyu, and E. Yildirim, “Perturbative unitarity bounds in composite 2-Higgs doublet models,” <https://arxiv.org/abs/1602.06437>.
  - [39] J. Mrazek, A. Pomarol, R. Rattazzi, M. Redi, J. Serra, and A. Wulzer, “The other natural two Higgs doublet model,” *Nuclear Physics B*, vol. 853, no. 1, 2011.
  - [40] E. Bertuzzo, T. S. Ray, H. de Sandes, and C. A. Savoy, “On composite two Higgs doublet models,” *Journal of High Energy Physics*, vol. 2013, article 153, 2013.
  - [41] M. Low, A. Tesi, and L. T. Wang, “Twin Higgs mechanism and a composite Higgs boson,” *Physical Review D*, vol. 91, article 095012, 2015.
  - [42] R. Barbieri, D. Greco, R. Rattazzi, and A. Wulzer, “The composite twin Higgs scenario,” *Journal of High Energy Physics*, vol. 2015, article 161, 2015.
  - [43] R. Contino, “A holographic composite Higgs model,” <https://arxiv.org/abs/hep-ph/0609148>.
  - [44] A. Carmona and F. Goertz, “A naturally light Higgs without light top partners,” *Journal of High Energy Physics*, vol. 2015, article 2, 2015.
  - [45] C. Csaki, T. Ma, and J. Shu, “Maximally symmetric composite Higgs models,” *Physical Review Letters*, vol. 119, article 131803, 2017.
  - [46] B. Gripaios, A. Pomarol, F. Riva, and J. Serra, “Beyond the minimal composite Higgs model,” *Journal of High Energy Physics*, vol. 904, p. 70, 2009.
  - [47] G. Ferretti, “UV completions of partial compositeness: the case for a SU (4) gauge group,” *Journal of High Energy Physics*, vol. 2014, article 142, 2014.
  - [48] M. Gillioz, R. Grober, C. Grojean, M. Muhlleitner, and E. Salvioni, “Higgs low-energy theorem (and its corrections) in composite models,” *Journal of High Energy Physics*, vol. 2012, article 4, 2012.
  - [49] V. Barger, P. Langacker, M. McCaskey, M. J. Ramsey-Musolf, and G. Shaughnessy, “CERN LHC phenomenology of an extended standard model with a real scalar singlet,” *Physical Review D*, vol. 77, article 035005, 2008.
  - [50] G. C. Branco, P. M. Ferreira, L. Lavoura, M. N. Rebelo, M. Sher, and J. P. Silva, “Theory and phenomenology of two-Higgs-doublet models,” *Physics reports*, vol. 516, pp. 1–102, 2012.
  - [51] G. Cacciapaglia, H. Cai, A. Deandrea, and A. Kushwaha, “Composite Higgs and dark matter model in SU (6)/SO (6),” *Journal of High Energy Physics*, vol. 2019, article 35, 2019.
  - [52] D. Croon, V. Sanz, and J. Setford, “Goldstone inflation,” *Journal of High Energy Physics*, vol. 2015, article 20, 2015.
  - [53] D. Croon, V. Sanz, and E. R. M. Tarrant, “Reheating with a composite Higgs,” <https://arxiv.org/abs/1507.04653>.
  - [54] J. R. Espinosa, B. Gripaios, T. Konstandin, and F. Riva, “Electroweak baryogenesis in non-minimal composite Higgs models,” *Journal of Cosmology and Astroparticle Physics*, vol. 2012, 2012.
  - [55] R. S. Gupta, V. V. Khoze, and M. Spannowsky, “Small instantons and the strong CP problem in composite Higgs models,” *Physical Review D*, vol. 104, no. 7, article 075011, 2021.
  - [56] M. Gorbahn, J. M. No, and V. Sanz, “Benchmarks for Higgs effective theory: extended Higgs sectors,” *Journal of High Energy Physics*, vol. 2015, article 36, 2015.
  - [57] V. Sanz and J. Setford, “Composite Higgses with seesaw EWSB,” *Journal of High Energy Physics*, vol. 2015, pp. 1–19, 2015.
  - [58] J. F. Gunion and H. E. Haber, “CP-conserving two-Higgs-doublet model: the approach to the decoupling limit,” *Physical Review D*, vol. 67, article 075019, 2003.
  - [59] A. Banfi, A. Martin, and V. Sanz, “Probing top-partners in Higgs+ jets,” *Journal of High Energy Physics*, vol. 2014, article 53, 2014.
  - [60] A. Banfi, B. M. Dillon, W. Ketaiam, and S. Kvedaraitė, “Composite Higgs at high transverse momentum,” *Journal of High Energy Physics*, vol. 2020, article 89, 2020.
  - [61] A. Banfi, A. Bond, A. Martin, and V. Sanz, “Digging for top squarks from Higgs data: from signal strengths to differential



- distributions,” *Journal of High Energy Physics*, vol. 2018, article 171, 2018.
- [62] J. de Blas, J. C. Criado, M. Perez-Victoria, and J. Santiago, “Effective description of general extensions of the standard model: the complete tree-level dictionary,” *Journal of High Energy Physics*, vol. 2018, article 109, 2018.
  - [63] H. L. Li, L. X. Xu, J. H. Yu, and S. H. Zhu, “EFTs meet Higgs nonlinearity, compositeness and (neutral) naturalness,” *Journal of High Energy Physics*, vol. 2019, article 10, 2019.
  - [64] J. Ellis, M. Madigan, K. Mimasu, V. Sanz, and T. You, “Top, Higgs, diboson and electroweak fit to the standard model effective field theory,” *Journal of High Energy Physics*, vol. 2021, article 279, 2021.
  - [65] ATLAS Collaboration, “Combination of the searches for pair-produced vector-like partners of the third-generation quarks at  $\sqrt{s} = 13$  TeV with the ATLAS detector,” <https://arxiv.org/abs/1808.02343>.
  - [66] CMS Collaboration, “Search for vector-like quarks in events with two oppositely charged leptons and jets in proton–proton collisions at  $\sqrt{s} = 13$  TeV,” *The European Physical Journal C*, vol. 79, no. 4, article 364, 2019.
  - [67] CMS Collaboration, “Search for vector-like T and B quark pairs in final states with leptons at  $\sqrt{s} = 13$  TeV,” *Journal of High Energy Physics*, vol. 2018, article 177, 2018.
  - [68] CMS Collaboration, “Search for pair production of vector-like quarks in the  $b\bar{W}bW$  channel from proton-proton collisions at  $\sqrt{s} = 13$  TeV,” <https://arxiv.org/abs/1710.01539>.
  - [69] CMS Collaboration, “Search for Pair Production of Vector-Like Quarks in the Fully Hadronic Channel,” <https://cds.cern.ch/record/2667230>.
  - [70] J. A. Aguilar-Saavedra, R. Benbrik, S. Heinemeyer, and M. Pérez-Victoria, “Handbook of vectorlike quarks: mixing and single production,” *Physical Review D*, vol. 88, article 094010, 2013.
  - [71] C. K. Khosa and V. Sanz, “On the impact of the LHC Run2 data on general composite Higgs scenarios,” <https://arxiv.org/abs/2102.13429>.